8-12-2024

Layered Naba2m3q3(q2) (M = Cu or Ag; Q = S or Se) Chalcogenides and Local Ordering in Their Mixed-Anion Compositions

Ayat Tassanov
The Pennsylvania State University

Huiju Lee
Portland State University

Yi Xia
Portland State University, yxia@pdx.edu

James M. Hodges
The Pennsylvania State University

Citation Details

Tassanov, A., Lee, H., Xia, Y., & Hodges, J. M. (2024). Layered NaBa2M3Q3(Q2) (M = Cu or Ag; Q = S or Se) Chalcogenides and Local Ordering in Their Mixed-Anion Compositions. Inorganic Chemistry, 63(34), 15584–15591.

Layered $NaBa_2M_3Q_3(Q_2)$ (M = Cu, Ag; Q = S, Se) Chalcogenides and Local Ordering in Their Mixed-Anion Compositions

Ayat Tassanov[†], Huiju Lee[§], Yi Xia[§], and James M. Hodges[†*]

[†] Department of Chemistry, The Pennsylvania State University, University Park, Pennsylvania 16802, United States.

[§] Department of Mechanical and Materials Engineering, Portland State University, Portland, Oregon 97201, United States.

KEYWORDS. Chalcogenides, Mixed-Anion, Crystal Structure, Raman Spectroscopy

ABSTRACT: Three new $NaBa_2M_3Q_3(Q_2)$ (M = Ag, Cu; Q = S, Se) chalcogenides were prepared using solid-state methods and structurally characterized using single-crystal X-ray diffraction. $NaBa_2Ag_3Se_3(Se_2)$ and $NaBa_2Cu_3Se_3(Se_2)$ crystallize in the monoclinic $C2/m$ space group and have a two-dimensional structure composed of edge-sharing $MSe_{4/4}$ tetrahedra separated by Na^+ and Ba^{2+} cations, along with $(Se_2)^{2-}$ dimers at the center of the spacings between $[M_3Se_3]^{3-}$ slabs. $NaBa_2Ag_3S_3(S_2)$ adopts a related structure with the $C2/m$ space group but has additional, crystallographically distinct Ag atoms in the $[Ag_3S_3]^{3-}$ layer that are linearly coordinated. $NaBa_2Ag_3Se_3(Se_2)$ and $NaBa_2Ag_3S_3(S_2)$ have indirect band gaps measured to be 1.2 eV and 1.9 eV, respectively, which is supported by band structures calculated using density functional theory. Mixed-anion $NaBa_2Cu_3Se_{5-x}S_x$ compositions were prepared to probe for the presence of anion ordering and heteronuclear $(S\text{-}Se)^{2-}$ dimers. Structural analyses of the sulfoselenides indicate selenium preferentially occupies the Q-Q dimer sites, while Raman spectroscopy reveals a mixture of (S_2), (Se_2), and heteronuclear (S-Se) units in the sulfur-rich products. The local ordering of the chalcogens is rationalized using simple bonding concepts and adds to a growing framework for understanding ordering phenomena in mixed-anion systems.

INTRODUCTION

The chalcogenides are a versatile class of solids that underpin various energy-related applications including photovoltaics,[1] catalysis,[2] and thermoelectrics.[3] They tend to have semiconducting properties with narrower band gaps and lower melting points than their oxide cousins. This allows for direct synthesis using high-temperature solid-state reactions and makes them ideally suited for substitutional studies. Additionally, unlike oxides, the chalcogens (Q = S, Se, Te) readily catenate into a rich assortment of polychalcogenide anions.[4] The length, charge, and connectivity of these polychalcogenide building blocks are highly variable, depending on both the metals they are coupled with and the conditions of the synthesis.[5-7] The structural diversity and tunable properties of metal chalcogenides continue to make them an active area for exploratory efforts and the discovery of new phenomena.

Copper and silver chalcogenides are a unique subclass of solids with electronic and thermal transport properties that have garnered interest in the field of thermoelectrics.[8-10] M-Q bonding (M = Cu, Ag) in these compounds involves chalcogen p orbitals and high-lying metal d orbitals with similar energies, which promotes greater p-d hybridization than with other transitional metals.[11] As a consequence, these materials have valence bands with large dispersions, significant metal character, and high carrier mobilities.[12, 13] Copper and silver are formally monovalent cations in chalcogenide frameworks and adopt many of the same structure types. Typically, the metal centers in these systems are in either distorted tetrahedral or trigonal coordination geometry.[14] Linear coordination is also possible but less prevalent than in the heavier Au congeners. Multinary systems containing electropositive alkali metals often crystallize in two-dimensional structure types, where covalent $[M_xQ_y]^{n-}$ slabs are separated by layers of counterbalancing cations.[15-18] The cation sublattices in these layered compounds are tunable and can be remarkably dynamic, making them useful in various applications and an effective platform for fundamental studies.[19] For example, dimensionally reduced KAg_3Se_2 has a suppressed superionic phase transition when compared to its three-dimensional Ag_2Se binary analogue,[20, 21] while the layered $AgCrSe_2$ ternary exhibits liquid-like thermal conductivity due to unique phonon scattering mechanisms that are correlated with the presence of disordered Ag^+ cations.[22] Conversely, divalent alkaline-earth cations are less mobile in layered structures but have other useful functionalities and are more likely to have $(Q_2)^{2-}$ dimeric anions.[23, 24] Disulfide and diselenide anions can undergo reversible redox processes and are emerging as structural motifs in cathode materials used in next-generation battery technologies.[25-27]

Group 11 (Cu, Ag) chalcogenides containing both alkali and alkaline-earth metals can have unique structural features and combined functionalities, but are less explored. Here, we report three new $NaBa_2M_3Q_3(Q_2)$ (M = Cu, Ag; Q = S, Se) compounds, including the first two examples in the

Na-Ba-Ag-Q quaternary spaces. The samples were prepared using high-temperature solid-state reactions of stoichiometric amounts of the elemental precursors. $NaBa_2Ag_3Se_3(Se_2)$ and $NaBa_2Cu_3Se_3(Se_2)$ crystallize in the $C2/m$ space group and are isostructural with $NaBa_2Cu_3S_3(S_2)$, a p-type degenerate semiconductor.[28] Their layered structures are composed of edge-sharing $MSe_{4/4}$ tetrahedra that form anionic $[M_3Se_3]^{3-}$ slabs that are counterbalanced by Na^+ and Ba^{2+} cations, with an additional layer of $(Se_2)^{2-}$ dimers at the center of the spacing. We find that $NaBa_2Ag_3S_3(S_2)$ crystallizes in a related, but unique structure type with distinct, linearly coordinated Ag atoms in the $[Ag_3S_3]^{3-}$ slab. UV-Vis spectroscopy and the corresponding Tauc plots show that $Na_2Ba_2Ag_3Se_3(Se_2)$ and $Na_2Ba_2Ag_3S_3(S_2)$ have indirect optical band gaps of 1.2 eV and 1.9 eV, respectively. Band structures calculated using density functional theory (DFT) corroborate the experimental data and the partial density of states (pDOS) for $Na_2Ba_2Ag_3S_3(S_2)$ indicate the linearly coordinated Ag atoms do not contribute to the band edges. In all of the reported compounds, the pDOS calculations indicate that the conduction band minimums are dominated by orbital contributions from the $(Q_2)^{2-}$ dichalcogen anions, which is an unexpected feature.

Our interest in mixed-anion materials motivated us to explore $NaBa_2Cu_3Se_{5-x}S_x$ sulfoselenide compositions to probe for the presence of local ordering and heteronuclear $(S\text{-}Se)^{2-}$ units. Although chalcogens tend to form solid solutions in simple binary crystal systems, ordering can occur in more complex structures that have multiple unique anion sites.[29] $NaBa_2Cu_3Se_{5-x}S_x$ samples were prepared using the same high-temperature solid-state protocol used to generate the single-anion end members and were characterized using single-crystal X-ray diffraction (SCXRD) and Raman spectroscopy. The structural analyses show varying degrees of mixed occupancy at the anion sites within the sulfoselenide products, with Se exhibiting a strong preference for the Q-Q dimer sites. The ordering is attributed to a combination of geometric and bonding factors. Raman spectroscopy was used to determine the chemical nature of the Q-Q anionic dimers and revealed a mixture of homonuclear (Se_2 and S_2) and heteronuclear Se-S dimers in the sulfur-rich compositions. Calculated phonon modes were used to model the Raman spectra and were found to be qualitatively in line with the experimental data and provided further evidence for the presence of $(S\text{-}Se)^{2-}$ dimeric anions. The report underscores the importance of using multiple complimentary techniques to characterize local ordering in complex solids, while also providing new insights for predicting the crystallographic locations that chalcogens will occupy in mixed-anion systems.

EXPERIMENTAL SECTION

Starting Materials. All materials were used as received. Copper chunks (Cu, 99.999%), selenium shot (Se, 99.999%), silver chunks (Ag, 99.999%), and sulfur flakes (S, 99.999%) were purchased from American Elements. Barium metal (Ba, 99%) was purchased from Thomas Scientific. Sodium chunks (Na, 98%) were purchased from Fisher Scientific). Chemical manipulations were performed inside a nitrogen-filled glovebox.

Synthesis. All of the $NaBa_2M_3Q_3(Q_2)$ (M = Cu, Ag; Q = S, Se) compounds were prepared through high-temperature reaction of elemental precursors in carbon-coated fused silica tubes that were flame-sealed under dynamic vacuum. In a typical 1.0 g reaction, stoichiometric amounts of precursors for a targeted product were weighed in a N_2-filled glovebox and loaded into a carbon-coated fused silica tube with an inner diameter of 9 mm. The tubes were evacuated to a pressure of $\sim 1 \times 10^{-3}$ Torr and then flame-sealed. The sealed tubes were then placed in a box furnace and heated to 450°C over 4 h, and then soaked at that temperature for 5 h, after which the furnace was ramped to 800°C in 3.5 h, where it dwelled for 24 h. Upon radiatively cooling, the tubes were opened in a N_2-filled glovebox to prevent oxidation/hydrolysis of the products, which were observed to tarnish in air after 24 h. The resulting ingots were found to contain plate-like single crystals of the targeted $NaBa_2M_3Q_3(Q_2)$ compositions that were suitable for single-crystal X-ray diffraction. The samples were stored in oil prior to single-crystal X-ray diffraction analysis.

Characterization by X-ray Diffraction. Single crystals of $NaBa_2M_3Q_3(Q_2)$ (M = Cu, Ag; Q = S, Se) compounds were mounted on a nylon loop using paratone oil, then transferred to a Rigaku Oxford Synergy Custom system with HyPix-Arc 150 diffractometer operating at 40 kV and 30 mA. Frames were collected at 173K using Oxford Cryostream during data collection. The radiation source was Cu Kα radiation (λ =1.5406 Å) for all samples. Space-group assignments were based on systematic absences, normalized structure factor statistics (*E* statistics), agreement factors for equivalent reflections, and successful refinement of the structure. The structures were solved by direct methods, expanded through successive difference Fourier maps using SHELXT, and refined against all data using the SHELXL-2014 software package as implemented in Olex2. Weighted *R* factors, R_w, and all goodness-of-fit indicators are based on F^2. We note that the overall anion ratios extracted from SCXRD refinements for the $NaBa_2Cu_3Se_{5-x}S_x$ sulfoselenides deviated slightly from the nominal synthesis composition, which is attributed to some degree of incongruent melting. In all cases, the deviation was less than 10%.

Powder X-ray diffraction (pXRD) patterns of polycrystalline samples were collected on a Bruker D2 PHASER diffractometer at room temperature with Cu Kα radiation (λ = 1.5406 Å) operating at 40kV and 40mA.

Characterization by UV-Vis Spectroscopy. Optical absorption data for finely ground polycrystalline $NaBa_2Ag_3Se_3(Se_2)$, and $NaBa_2Ag_3S_3(S_2)$ samples were recorded in diffuse reflectance mode on a Shimadzu UV-3600 UV–vis-NIR spectrophotometer. $BaSO_4$ was used as a reflectance standard. The reflectance data were transformed to absorption using the Kubelka–Munk function, $F(R)$, defined as $(1\text{-}R)^2/2R$, where R is the diffuse reflectance. The corresponding Tauc plots were constructed by plotting $(h\nu F(R))^{1/2}$ vs $h\nu$, and the (indirect) band gaps were obtained by determining the onset of absorption.

Scanning Electron Microscopy. Scanning electron microscopy (SEM) imaging and energy-dispersive X-ray spectroscopy (SEM-EDS) were performed on a Verios G4 scanning electron microscope equipped with an FEM source.

Raman Spectroscopy. Raman spectra were collected on a LabRAM Soleil (Horiba) confocal spectrometer. An excitation wavelength of 532 nm was used, and the power was tested on all the material to make sure no beam damage occurs. A power of 6 mW was used for $NaBa_2Cu_3Se_3(Se_2)$ and $NaBa_2Cu_3S_3(S_2)$ samples since no damage was observed at this power. The $NaBa_2Cu_3Se_{5-x}S_x$ (x = 1, 2.8, 4) samples showed some power damage at 6 mW, hence the power was set to 1.2 mW. The spectra were recorded using a 50× objective (Numerical aperture of 0.6 and working distance of 11.0 mm). The grating used for the measurement was 1800 groove/mm. The signal was collected by using a Syncerity 1024x256OE (Horiba) CCD detector. The exposure time was set to 20 s to prevent damage to the sample. A confocal hole of 200 um was used due to the homogeneity of the sample. The spectra were collected at multiple spots to confirm the uniformity of the samples.

Density Functional Theory Calculations. All the density functional theory (DFT) calculations[30, 31] in this paper were carried out using Vienna Ab-initio Simulation Package (VASP).[32-34] A projector-augmented wave (PAW)[35] pseudopotentials method and plane-wave basis sets were used with Perdew-Burke-Ernzerhof (PBE)[36] of the generalized gradient approximation (GGA)[37] as an exchange-correlation functional. For the band structure and the density of states calculations, self-consistent DFT calculations were firstly performed, and the cutoff energy of 350 eV and 400 eV were used for the Ag compounds and Cu compounds, respectively. The Brillouin zone was evenly sampled using a k-spacing of 0.3 and the energies were converged to less than 10^{-5} eV. After the self-consistent calculations, the band structures and the density of states were calculated using the HSE06[38] hybrid functional. In order to calculate the Raman active phonon modes, Phonopy[39] and Phonopy-Spectroscopy[40] software packages were used, and the phonon calculations were implemented using primitive cells. For the phonon calculations, the cutoff energy of 520 eV and the k-spacing of 0.15 were used, and the energies and the forces convergence criteria were set to 10^{-8} eV and 10^{-3} eV/Å, respectively. Eigenvectors and eigenvalues at Γ-point and irreducible representations of phonon modes were calculated using Phonopy. By referring to character tables for the corresponding point group of each compound, we extracted Raman active modes. The unit of Raman shift was converted from THz used in the phonon calculations to cm^{-1} to compare them with experimental results. It is worth noting that we find structural relaxation of $NaBaCu_3Se_3(Se_2)$ gives rise to unreasonably large interatomic distances between Se atoms in Se-Se dimer (Exp. 2.398 Å vs. Calc. 2.669 Å) and thus significantly underestimated phonon frequencies. We further confirmed this finding by verifying against different exchange correlation functionals. Therefore, we adopted the experimental structure for $NaBaCu_3Se_3(Se_2)$ Raman spectra calculations. The band structures present in the main text were also computed using the experimental structures. Note that we also computed the band structures using theoretically relaxed structures but did not find significant differences in the shape of band structures and band gaps.

RESULTS AND DISCUSSION

$NaBa_2Ag_3Se_3(Se_2)$, $NaBa_2Cu_3Se_3(Se_2)$, and $NaBa_2Ag_3S_3(S_2)$ were synthesized directly using high-temperature solid-state reactions of stoichiometric amounts of elemental precursors. Briefly, the appropriate amount of elemental Na, Ba, Ag(Cu), Se(S) were placed in a carbon-coated fused-silica tube and evacuated to ~10^{-3} Torr and then flame sealed under dynamic vacuum. The reaction vessels were heated to 450°C and held for 5h, then ramped to 800°C and soaked for 24h. Upon radiative cooling, the $NaBa_2Ag_3Se_3(Se_2)$ and $NaBa_2Cu_3Se_3(Se_2)$ ingots yielded black plate-like crystals that were suitable for single crystal X-ray diffraction. $NaBa_2Ag_3S_3(S_2)$ reactions yielded plate-like crystals with orange to yellow color. Single-crystal diffraction data for $NaBa_2Cu_3Se_3(Se_2)$, $NaBa_2Ag_3Se_3(Se_2)$, and $NaBa_2Ag_3S_3(S_2)$ crystals are shown in Table S1 along with information regarding their structural refinements. Full structural details and anisotropic displacement parameters can be found in the Supporting Information (Tables S2-S16).

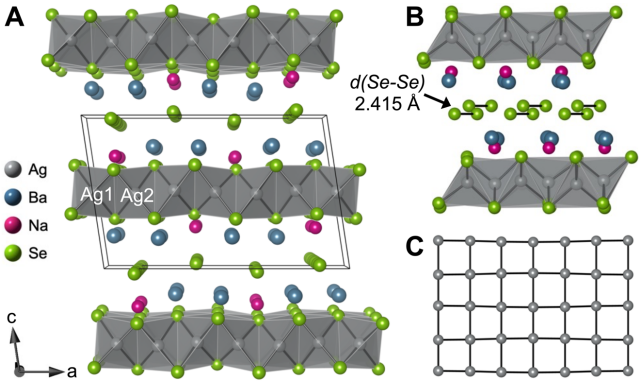

Figure 1. (A) Crystal structure of $NaBa_2Ag_3Se_3(Se_2)$ viewed along the b axis showing layers of edge-sharing $AgSe_4$ tetrahedra separated by Na^+, Ba^{2+}, and $(Se_2)^{2-}$ dimers, which are better visualized in the alternate view shown in (B). The Ag sublattice exhibits a square-net arrangement when viewed along the c-axis (C).

$NaBa_2Ag_3Se_3(Se_2)$ and $NaBa_2Cu_3Se_3(Se_2)$ crystallize in the monoclinic $C2/m$ space group and are isostructural with $NaBa_2Cu_3S_3(S_2)$. The crystallographic asymmetric unit for $NaBa_2Ag_3Se_3(Se_2)$ contains one Na atom, two Ba atoms, two Ag atoms, and 4 Se atoms. The two-dimensional structure has edge-sharing $AgSe_{4/4}$ tetrahedra that form anionic $[Ag_3Se_3]^{3-}$ slabs separated by Na^+ and Ba^{2+} cations, with $[Se_2]^{2-}$ dimeric anions located at the center of the spacing between the slabs (Figure 1A). The $[Se_2]^{2-}$ dimer units do not interact directly with the Cu-S layer and accordingly, the chemical formula for the compound is best described as $NaBa_2Ag_3Se_3(Se_2)$. The rotated view of the structure in Figure 1B shows a better visualization of the $[Se_2]^{2-}$ dimers at the center of the spacing, with Se-Se bond distances of 2.413 Å. The Ag sublattice is a two-dimensional square net as illustrated in Figure 1C and has Ag-Ag distances ranging from 2.8493 Å to 3.1317 Å. We note that several of the Ag-Ag distances are shorter than those found in elemental fcc Ag, which is not uncommon in layered Ag chalcogenides. The $NaBa_2Cu_3Se_3(Se_2)$ structure is shown in Figure S1A-B and is found to have shorter Se-Se bonds of 2.397 Å in the dimer unit. The square net Cu sublattice shows greater

distortion than in the Ag analogue, with Cu-Cu distances ranging from 2.694 Å to 3.085 Å, which are longer than those found in fcc Cu.

The edge-sharing $MSe_{4/4}$ tetrahedra are distorted in $NaBa_2Ag_3Se_3(Se_2)$ and $NaBa_2Cu_3Se_3(Se_2)$ as illustrated in the bond distance histograms shown in Figures S1B-C. In both cases, the M(1)Se_4 tetrahedra show a greater degree of distortion than the M(2)Se_4 unit. For $NaBa_2Ag_3Se_3(Se_2)$, Ag(1) has two short Ag1-Se2 bonds with distances of 2.6929 Å and two longer Ag1-Se3 bonds of 2.8164 Å. The Ag(2)Se_4 tetrahedra are less distorted, with Ag2-Se bond lengths of 2.7106 Å, 2.7601 Å, 2.7671 Å, and 2.8428 Å. Similarly, for $NaBa_2Cu_3Se_3(Se_2)$, Cu(1)Se4 has two short Cu1-Se2 bonds with distances of 2.4925 Å and two Cu1-Se3 bonds of 2.5471 Å. Again, the Cu(2)Se_4 is less distorted with Cu2-Se distances of 2.5023 Å, 2.5243 Å, 2.5272 Å, and 2.5588 Å. We note that the Se1 anion is coordinated to four Cu atoms with bond distances ranging from 2.4925 Å to 2.5023 Å, which are significantly shorter than four-coordinate Se2, with bonds ranging from 2.5243 Å to 2.5588 Å, and the four-coordinate Se3 atom with bonds ranging from 2.5272 Å to 2.5471 Å. The anion ordering in the $NaBa_2Cu_3Se_{5-x}S_x$ sulfoselenide products, which is described below, is attributed to the different local chemistry at the 3 unique Q sites in the single-anion end members.

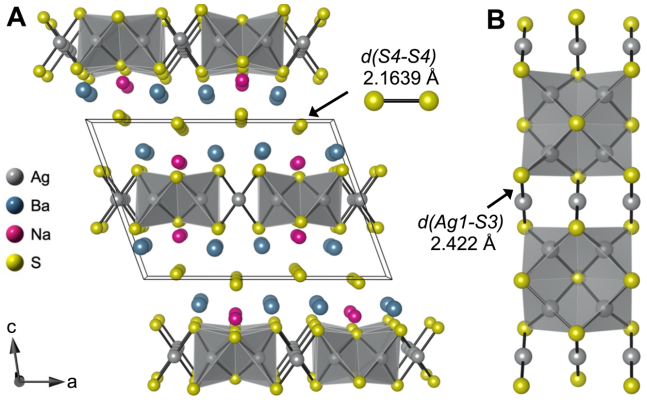

Figure 2. Crystal structure of $NaBa_2Ag_3S_3(S_2)$ viewed along the (A) b-axis showing two-dimensional slabs composed of both $AgSe_4$ tetrahedra and linearly coordinated Ag, which are separated by Na^+, Ba^{2+}, and $(S_2)^{2-}$ dimers. (B) Section of AgS layer viewed from c-axis, showing alternation of tetrahedral and linearly coordinated Ag.

$NaBa_2Ag_3S_3(S_2)$ crystallizes in a similar structure as $NaBa_2Ag_3Se_3(Se_2)$ with the $C2/m$ space group but contains both tetrahedral and linear coordinated Ag atoms in the $[Ag_3S_3]^{3-}$ layer. $NaBa_2Ag_3S_3(S_2)$ has a crystallographic asymmetric unit with one Na atom, two Ba atoms, three Ag atoms, and 4 S atoms. Figure 2A displays the structure viewed along the b-axis showing two-dimensional layers composed of chains of edge-sharing Ag(3)S_4 tetrahedra connected by linearly coordinated Ag(1) and Ag(2) atoms. The structure viewed along the c-axis (Figure 2B) shows the linear Ag(1)S_2 and Ag(2)S_2 units, which alternate along the b-axis and are nearly perpendicular. The Ag(3)S_4 bond distances range from 2.623 Å to 2.7382 Å, while Ag(1)S_2 and Ag(2)S_2 have two Ag-S bonds of 2.4216 Å and 2.4223 Å, respectively, which are in line with literature values reported for tetrahedral and linear Ag-S bonds, respectively.[41] The Ag sublattice in $NaBa_2Ag_3S_3(S_2)$ shows greater complexity than the Se analogue. Ag(1) interacts with six adjacent Ag atoms with distances ranging from 2.9085 Å to 2.9702 Å, Ag(2) with six Ag atoms with distances ranging from 2.9085 Å to 2.9709 Å, while Ag(3) interacts with five Ag atoms with distances ranging from 2.9071 Å to 3.1866 Å. Similar to the selenium analogue, the $[Ag_3S_3]^{3-}$ layer is separated by Na^+ and Ba^{2+} cations with $[S_2]^{2-}$ dimers residing at the center of the spacing. The S-S bond distance is 2.1639 Å, which is slightly longer than the S-S bond distance reported in $NaBa_2Cu_3S_3(S_2)$.

Powder X-ray diffraction (pXRD) was used to determine the purity of the bulk samples, and the diffractograms for $NaBa_2Ag_3Se_3(Se_2)$, $NaBa_2Cu_3Se_3(Se_2)$, and $NaBa_2Ag_3S_3(S_2)$ are shown in Figures S2A-C along with the corresponding simulated patterns from the SCXRD analyses. In each case, the intensity of the (h00) reflections are enhanced due to preferred orientation. Unidentified peaks attributed to minor impurities are seen in $NaBa_2Cu_3Se_3(Se_2)$ and $NaBa_2Ag_3S_3(S_2)$ diffractograms and marked with an asterisk. Scanning electron microscopy (SEM) images for each sample is show in Figures S2D-E. The SEM images show plate-like crystals that is expected in materials that have layered structure types. SEM coupled with energy dispersive spectroscopy (SEM-EDS) provides semi-quantitative elemental analysis of the crystals and is consistent with the compositions from the SCXRD refinements.

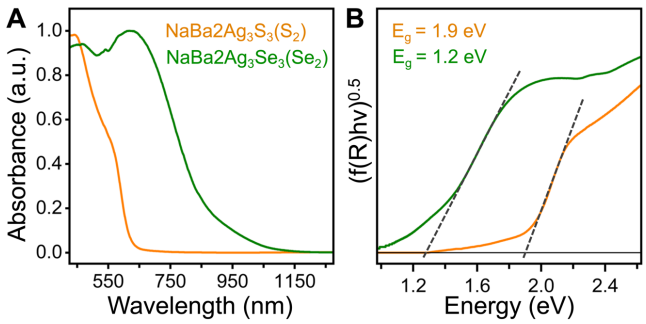

Figure 3. (A) UV-Vis absorption and (B) corresponding Tauc plots for $NaBa_2Ag_3Se_3(Se_2)$ and $NaBa_2Ag_3S_3(S_2)$, which have green and orange profiles, respectively.

Room-temperature UV-Vis absorption data for the bulk powders was collected in reflectance mode and is shown in Figure 3A. The $NaBa_2Ag_3Se_3(Se_2)$ and $NaBa_2Ag_3S_3(S_2)$ absorption spectra are shown in green and orange, respectively. The corresponding Tauc plots are shown in Figure 3B and indicate the compounds are semiconductors with indirect band gaps of 1.2 eV for $NaBa_2Ag_3Se_3(Se_2)$ and 1.9 eV for $NaBa_2Ag_3S_3(S_2)$. Accurate absorption spectra were not obtained for the $NaBa_2Cu_3Se_3(Se_2)$ sample since it was outside the range of the spectrometer, but was calculated to have an indirect band gap of 0.65 eV as described below.

To better understand the electronic properties of the materials, we computed the band structure and atom-decomposed density of states (DOS) for $NaBa_2Ag_3Se_3(Se_2)$, $NaBa_2Ag_3S_3(S_2)$, and $NaBa_2Cu_3Se_3(Se_2)$, as shown in Figures 4A, 4B, and S3, respectively. Specifically, we employed HSE06, a hybrid functional for describing the exchange-

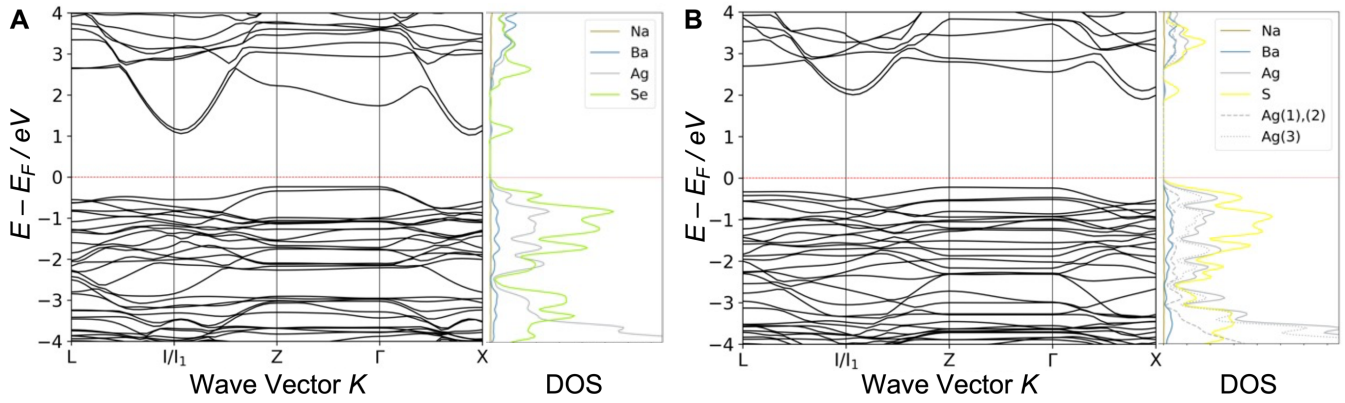

Figure 4. DFT-calculated electronic structure along with atom-decomposed DOS for (A) $NaBa_2Ag_3Se_3(Se_2)$ and (B) $NaBa_2Ag_3Se_3(Se_2)$, where the Fermi level has been set to 0 eV and is denoted by red dashed lines. The orbital character at the CBM is composed of chalcogen p-orbitals, while the VBM has contributions from both chalcogens and d-orbitals from tetrahedral Ag.

correlation energy in density functional theory, to provide a more accurate prediction of the band gaps. We see that all three compounds are expected to have indirect band-gaps, with values of 1.2 eV and 2.1 eV for $NaBa_2Ag_3Se_3(Se_2)$ and $NaBa_2Ag_3S_3(S_2)$, which are in good agreement with the experimentally determined values. $NaBa_2Cu_3Se_3(Se_2)$ is predicted to have an indirect band gap of 0.65 eV. In all three compounds, the conduction band minimum (CBM) is found to be isotropically dispersive, while the valence band maximum (VBM) exhibits strong anisotropy, that is, the band dispersion is extremely flat along the Z-Γ direction and becomes dispersive when moving away from Z/Γ points. The corresponding DOS reveals that the states near the VBM are primarily composed of *d* orbitals from Ag/Cu atoms and *p* orbitals of S/Se atoms, while the states near CBM display S/Se character. Figure 4B shows the different contributions to the pDOS from linearly coordinated Ag(1), Ag(2), and tetrahedrally coordinated Ag(3) atoms, indicating that Ag(3) atoms play a more critical role in the VBM.

Metals in mixed-anion environments can have unique coordination geometries and distinctive properties not found in their single-anion analogues. Mixed-chalcogen compounds are a particularly interesting class of solids with electronic properties that can be fine-tuned by adjusting the ratio of chalcogen anions. Although chalcogens will form solid solutions in simple crystal systems, ordering does occur when the anion sublattice has multiple sites with distinct local chemistries. Accordingly, we prepared the $NaBa_2Cu_3Se_{5-x}S_x$ sulfoselenides to probe for local ordering and additionally, the presence of heteroatom (Se-S) dimers units, which have not been reported to the best of our knowledge. We note that attempts to synthesize the mixed-anion $NaBa_2Ag_3Se_{5-x}S_x$ compositions were unsuccessful, yielding mixtures of the sulfide and selenide end members with minimal chalcogen mixing.

The $NaBa_2Cu_3Se_{5-x}S_x$ (x = 1, 2.8, 4, 5) samples were prepared using the same high-temperature solid-state reactions described for the single anion compounds and structurally characterized with SCXRD. Refinement details and anisotropic displacement parameters can be found in the Supporting Information (Tables S17-S34). The composition of the x = 2.8 compound deviated slightly from nominal composition from the synthesis, which is attributed to incongruent melting. The corresponding pXRD are shown in Figure S4, along with optical images of the plate-like crystals used for Raman spectroscopy. All of the peaks in the simulated patterns are accounted for in the experimental powder diffractograms with some enhancement in the (h00) reflections due to preferred orientation. Minor impurity peaks indexed to BaSe are attributed to incongruent melting in the mixed-anion compositions.

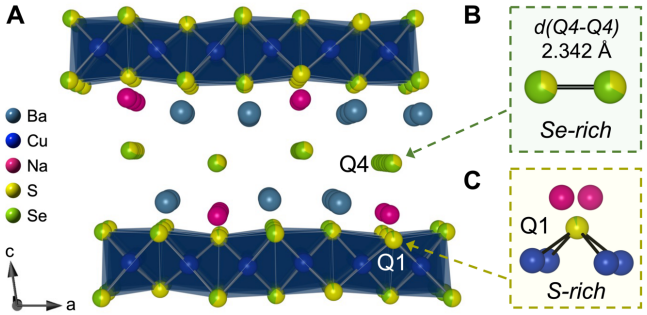

Figure 5. (A) Structure of $NaBa_2Cu_3Se_{2.2}S_{2.8}$ sulfoselenide showing varying degrees of S/Se mixed-occupancy at the different anion sites. (B) Q4-Q4 dimers with Se-rich mixed-occupancy and (C) S-rich mixed-occupancy at the Q1 site.

We observe significant chalcogen ordering in each of the $NaBa_2Cu_3Se_{5-x}S_x$ products, where S and Se show preference for particular Wyckoff positions within the lattice. Figure 5A shows the structure of $NaBa_2Cu_3Se_{2.2}S_{2.8}$, which adopts the monoclinic $C2/m$ space group and exemplifies the ordering trends seen throughout the series. Here, although the compound has an overall anion composition of 46% Se and 54% S, each of the 4 unique Q sites deviates from the values expected in a solid solution. The Q1 and Q4 sites show the largest deviation, with S-rich Q1 site having 95% S occupancy and the Se-rich Q4 site showing 67% Se occupancy. We rationalize the prevalence of S at the Q1 site through careful examination of the $NaBa_2Cu_3Q_3(Q_2)$ end members, where the Q1 sites have the shortest Q-Cu bond lengths. Additionally, these sites interact strongly with two counterbalancing Na^+ cations (Figure 5C), which cause a puckering of the two-dimensional slabs. Hence, S shows a preference for the site due to a combination of geometric and bonding factors, the latter rationalized according to hard-soft acid-base theory. The strong preference for Se to occupy the Q4 dimeric $(Q\text{-}Q)^{2-}$ anion sites is also likely a

combination of factors. The dimeric anions sit at the center of the spacing between the layers, where there is more volume for the larger Se atoms. Likewise, the charge-density of the $(Se\text{-}Se)^{2-}$ units is lower than the $(S\text{-}S)^{2-}$, which could also play a role. The refined unit cell volumes from SCXRD analysis of the $NaBa_2Cu_3Se_{5-x}S_x$ (x = 1, 2.8, 4, 5) crystals is shown in Figure 6A. The volume decreases nearly linearly with increasing S content, in accordance with Vegard's law. In contrast, the associated change in Q-Q bond distance is not linear (Figure 6B), indicating Se preferentially occupies the Q4 site across the entire series.

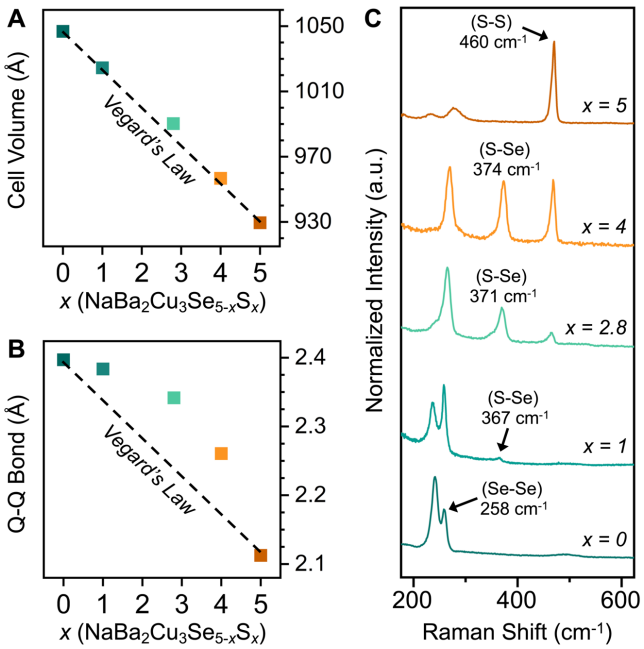

Figure 6. (A) Unit Cell volume as a function of x in $NaBa_2Cu_3Se_{5-x}S_x$ sulfoselenides showing nearly linear decrease across the series, in accordance with Vegard's law, while (B) Q-Q dimer bond distance deviates significantly due Se preference for the dimer sites. (C) Raman spectra for the $NaBa_2Cu_3Se_{5-x}S_x$ products, showing mixtures of Se-Se, S-S, and heteronuclear Se-S dimer units in the mixed-anion compositions.

The varying occupancies at Q4-Q4 dimer sites obtained from SCXRD data represents the average composition, which could be attributed to a either a mixture of homonuclear dimers (Se-Se, S-S), or homonuclear and heteronuclear dimers (Se-S). Raman spectroscopy was used to gain further insight into the chemical nature of the Q4-Q4 anions and the spectra are shown in Figure 6C. $NaBa_2Cu_3S_3(S_2)$ was synthesized for comparison using the same high-temperature methods described above. The $NaBa_2Cu_3Se_3(Se_2)$ spectra (x = 0) has peaks at 258 cm^{-1} and 242 cm^{-1}, both of which are in the range of previously reported values for Se-Se stretching modes from $(Se_2)^{2-}$ units. Accordingly, it is difficult to say conclusively which peak is from the Se-Se stretching mode. DFT calculations (described below) suggest that the peak at 258 cm^{-1} is attributed to the Se-Se stretch, and the lower frequency peak at 242 cm^{-1} is likely from Cu-Se vibrational modes. The spectra for $NaBa_2Cu_3Se_4S$ (x = 1) has the similar peaks at 241 cm^{-1} and 258 cm^{-1}, with an additional minor peak at 367 cm^{-1} that is consistent with a heteronuclear Se-S stretching mode.[42] In comparison, the $NaBa_2Cu_3Se_{2.2}S_{2.8}$ (x = 2.8) sulfoselenide has an enhanced Se-S peak at 369 cm^{-1} and the emergence of a peak at 467 cm^{-1}, which is in consistent with S-S stretching modes. Accordingly, the Q4-Q4 dimer shown in Figure 5B likely represents a mixture of Se-Se, Se-S, and S-S dimers. The spectra for $NaBa_2Cu_3SeS_4$ (x = 2.8) indicate this composition contains the same three dimers, but with higher concentrations of Se-S and S-S. The $NaBa_2Cu_3S_3(S_2)$ end member (x = 5) shows a single S-S peak at approximately 470 cm^{-1}, as previously reported.

To better understand the vibrational properties, we computed phonon modes at the Brillouin center for $NaBaCu_3Se_3(Se_2)$ and $NaBaCu_3S_3(S_2)$ using their primitive cells. The computed phonon modes were then analyzed using group theory to identify the Raman active modes, as shown in Figure S5. We chose not to directly simulate the phonon modes for mixed chalcogen compounds due to the inherent challenges modeling partial occupancy. As shown in Figure S5A, the highest-lying Raman active phonon mode of $NaBaCu_3S_3(S_2)$ has a frequency of about 460 cm^{-1}, in very good agreement with the experimental values of about 470 cm^{-1}. Moreover, the visualized eigenvector of the corresponding phonon modes clearly reveals the nature of stretching of S-S dimers. Our detailed analysis of the eigenvectors of vibrational modes shows that modes with frequencies higher than 150 cm^{-1} are mainly associated with S vibrations. For $NaBaCu_3Se_3(Se_2)$, our simulated Raman active modes in Figure S6C show the highest-lying mode is associated with the Se-Se vibrations, in accordance with our earlier experimental assignment. Compared to the S compound, the Se compound shows drastically decreased vibrational frequencies, which is not unexpected due to the heavier mass of Se and weaker bonding within Se-Se dimers. Therefore, the simulations semi-quantitatively confirmed the experimentally measured Raman active modes, despite some underestimation of vibrational frequencies for $NaBaCu_3Se_3(Se_2)$.

CONCLUSIONS

Three new quaternary chalcogenides were generated using high-temperature solid-state synthesis and include the first reported compounds in the Na-Ba-Ag-Q quaternary space. The SCXRD analysis indicates the compounds all crystallize in the monoclinic $C2/m$ space group, including $NaBa_2Ag_3Se_3(Se_2)$ and $NaBa_2Cu_3Se_3(Se_2)$, which are isostructural systems composed of layers of edge-sharing $AgSe_{4/4}$ and $CuSe_{4/4}$ tetrahedra separated by Ba^{2+}, Na^{+}, and $(Se_2)^{2-}$ dimeric anions. The third $NaBa_2Ag_3S_3(S_2)$ sulfide compound shares the same stoichiometry but includes crystallographically distinct Ag atoms with linear coordination in the $[Ag_3Se_3]^{3-}$ layer. The asymmetric unit for $NaBa_2Ag_3S_3(S_2)$ has one Na atom, two Ba atoms, three Ag atoms, and 4 S atoms, with similar features as the quaternary selenides but with different bonding features and a unique structure. DFT-calculated band structures indicate the materials are indirect band gap semiconductors, which was experimentally confirmed for $NaBa_2Ag_3Se_3(Se_2)$ (band gap = 1.19 eV) and $NaBa_2Ag_3S_3(S_2)$ (band gap = 1.91 eV). The partial density of states shows that the VBM are composed of orbitals from the tetrahedrally coordinated metals and chalcogen anions, while the CBM is primarily at-

tributed to chalcogens from the (Q_2) dimer sites. Chalcogen ordering in the mixed-anion $NaBa_2Cu_3Se_4S$ and $NaBa_2Cu_3SeS_4$ sulfoselenides compositions are attributed to geometric constraints and the Raman spectra for $NaBa_2Cu_3SeS_4$ reveal the $(Q_2)^{2-}$ anions are a mixture of $(S_2)^{2-}$, $(Se_2)^{2-}$, and a rare example of heteroatomic $(S\text{-}Se)^{2-}$ dimeric units. We believe that local ordering in mixed-chalcogen materials plays an important, but underappreciated role in defining their properties. The degree of ordering is likely variable, and is defined by the synthetic conditions and the crystal chemistry of the parent structure. This report highlights the importance of using multiple complementary techniques to accurately describe the local chemistry in mixed-anion materials, while also offering guidelines for predicting when and how this phenomena will occur.

ASSOCIATED CONTENT

Supporting Information

The Supporting Information is available free of charge on the ACS Publications website.

Crystallographic data files for the structures in this paper are available by request to the Cambridge Crystallographic Data Centre (CCDC) in the form of crystallographic information files with associated CCDC numbers of 2307667 ($NaBa_2Cu_3Se_5$), 2307675 ($NaBa_2Ag_3S_5$), 2307668 ($NaBa_2Ag_3Se_5$), 2326693 ($NaBa_2Cu_3Se_4S$), 2326693 ($NaBa_2Cu_3Se_{2.2}S_{2.8}$), and 2326692 ($NaBa_2Cu_3SeS_4$). These data can be obtained free of charge from CCDC (https://www.ccdc.cam.ac.uk/); Optical images of $Na_2Ba_2Ag_3Se_3(Se_2)$, $Na_2Ba_2Ag_3S_3(S_2)$, and $Na_2Ba_2Cu_3Se_3(Se_2)$ crystals; pXRD, SEM, SEM-EDS, and full crystallographic tables for all reported $NaBa_2M_3Q_3(Q_2)$ (M = Cu, Ag; Q = S, Se) compounds (PDF)

AUTHOR INFORMATION

Corresponding Author

James M. Hodges – Department of Chemistry, Pennsylvania State university, University Park, Pennsylvania 16802, United States; orcid.org/0000-0002-2306-0845
Email: hodges@psu.edu

Author Contributions

The manuscript was written through contributions of all authors. All authors have given approval to the final version of the manuscript.

Notes

The authors declare no competing financial interest.

ACKNOWLEDGMENT

This work was supported in part by the Eberly College of Science and the Department of Chemistry at the Pennsylvania State University. Characterization was conducted at the Integrated Macromolecular and Small Molecule X-ray Crystallography Facility, and the Materials Characterization Lab, both at Penn State. The authors would like to thank Hemant Yennawar for assistance with structural characterization, and acknowledge support from National Institutes of Health through award #1S10OD028589-01 and #1S10RR023439-01 for X-ray instrumentation. H.L. and Y.X. acknowledge support from the US National Science Foundation through award #2317008 (phonon calculations).

REFERENCES

(1) Wu, X. High-efficiency polycrystalline CdTe thin-film solar cells. *Solar Energy* **2004**, *77* (6), 803-814.

(2) Benck, J. D.; Hellstern, T. R.; Kibsgaard, J.; Chakthranont, P.; Jaramillo, T. F. Catalyzing the Hydrogen Evolution Reaction (HER) with Molybdenum Sulfide Nanomaterials. *ACS Catalysis* **2014**, *4* (11), 3957-3971.

(3) Heremans, J. P.; Jovovic, V.; Toberer, E. S.; Saramat, A.; Kurosaki, K.; Charoenphakdee, A.; Yamanaka, S.; Snyder, G. J. Enhancement of Thermoelectric Efficiency in PbTe by Distortion of the Electronic Density of States. *Science* **2008**, *321* (5888), 554-557.

(4) Kanatzidis, M. G. Discovery-Synthesis, Design, and Prediction of Chalcogenide Phases. *Inorganic Chemistry* **2017**, *56* (6), 3158-3173.

(5) Sheldrick, W. S. Polychalcogenides. In *Handbook of Chalcogen Chemistry: New Perspectives in Sulfur, Selenium and Tellurium, Volume 1*, Wickleder, M. S., Devillanova, F., Du Mont, W.-W., Devillanova, F., Du Mont, W.-W. Eds.; Vol. 1; The Royal Society of Chemistry, 2013; p 0.

(6) Sheldrick, W. S.; Wachhold, M. Chalcogenidometalates of the heavier Group 14 and 15 elements. *Coordination Chemistry Reviews* **1998**, *176* (1), 211-322.

(7) Dorhout, P. K.; Ford, N. B.; Raymond, C. C. Understanding the polychalcogenides as building blocks to solid state materials: Speciation of polychalcogenides in solutions. *Coordination Chemistry Reviews* **2017**, *352*, 537-550.

(8) Lin, H.; Tan, G.; Shen, J.-N.; Hao, S.; Wu, L.-M.; Calta, N.; Malliakas, C.; Wang, S.; Uher, C.; Wolverton, C.; Kanatzidis, M. G. Concerted Rattling in $CsAg_5Te_3$ Leading to Ultralow Thermal Conductivity and High Thermoelectric Performance. *Angewandte Chemie International Edition* **2016**, *55* (38), 11431-11436.

(9) Ma, N.; Li, Y.-Y.; Chen, L.; Wu, L.-M. α-$CsCu_5Se_3$: Discovery of a Low-Cost Bulk Selenide with High Thermoelectric Performance. *Journal of the American Chemical Society* **2020**, *142* (11), 5293-5303.

(10) Assoud, A.; Thomas, S.; Sutherland, B.; Zhang, H.; Tritt, T. M.; Kleinke, H. Thermoelectric Properties of the New Polytelluride $Ba_3Cu_{14-\delta}Te_{12}$. *Chemistry of Materials* **2006**, *18* (16), 3866-3872.

(11) Woods-Robinson, R.; Han, Y.; Zhang, H.; Ablekim, T.; Khan, I.; Persson, K. A.; Zakutayev, A. Wide Band Gap Chalcogenide Semiconductors. *Chemical Reviews* **2020**, *120* (9), 4007-4055.

(12) Zeier, W. G.; Zevalkink, A.; Gibbs, Z. M.; Hautier, G.; Kanatzidis, M. G.; Snyder, G. J. Thinking Like a Chemist: Intuition in Thermoelectric Materials. *Angewandte Chemie International Edition* **2016**, *55* (24), 6826-6841.

(13) Vajenine, G. V.; Hoffmann, R. Compounds Containing Copper−Sulfur Layers: Electronic Structure, Conductivity, and Stability. *Inorganic Chemistry* **1996**, *35* (2), 451-457.

(14) Keane, P. M.; Lu, Y. J.; Ibers, J. A. Copper-containing Group IV and Group V chalcogenides. *Accounts of Chemical Research* **1991**, *24* (8), 223-229.

(15) Xia, Z.; Fang, H.; Zhang, X.; Molokeev, M. S.; Gautier, R.; Yan, Q.; Wei, S.-H.; Poeppelmeier, K. R. $CsCu_5Se_3$: A Copper-Rich Ternary Chalcogenide Semiconductor with Nearly Direct Band Gap for Photovoltaic Application. *Chemistry of Materials* **2018**, *30* (3), 1121-1126.

(16) Friedrich, D.; Quintero, M. A.; Hao, S.; Laing, C. C.; Wolverton, C.; Kanatzidis, M. G. $AInSn_2S_6$ (A = K, Rb, Cs)—Layered Semiconductors Based on the SnS_2 Structure. *Inorganic Chemistry* **2022**, *61* (34), 13525-13531.

(17) Pell, M. A.; Ibers, J. A. Layered Ternary and Quaternary Metal Chalcogenides. *Chemische Berichte* **1997**, *130* (1), 1-8. DOI: 10.1002/cber.19971300102 (acccessed 2023-09-26T19:47:10).

(18) Pomelova, T. A.; Delacotte, C.; Kuratieva, N. V.; Lemoine, P.; Cordier, S.; Park, S.; Guizouarn, T.; Pelletier, V.; Gautier, R.; Naumov, N. G. $Cs_2Ln_3CuS_8$ (Ln = La–Nd, Sm–Tb): Synthesis, Crystal Structure, and Magnetic and Optical Properties. *Inorganic Chemistry* **2023**, *62* (17), 6586-6597.

(19) Liu, H.; Shi, X.; Xu, F.; Zhang, L.; Zhang, W.; Chen, L.; Li, Q.; Uher, C.; Day, T.; Snyder, G. J. Copper ion liquid-like thermoelectrics. *Nature Materials* **2012**, *11* (5), 422-425.

(20) Rettie, A. J. E.; Ding, J.; Zhou, X.; Johnson, M. J.; Malliakas, C. D.; Osti, N. C.; Chung, D. Y.; Osborn, R.; Delaire, O.; Rosenkranz, S.; Kanatzidis, M. G. A two-dimensional type I superionic conductor. *Nature Materials* **2021**, *20* (12), 1683-1688.

(21) Rettie, A. J. E.; Malliakas, C. D.; Botana, A. S.; Hodges, J. M.; Han, F.; Huang, R.; Chung, D. Y.; Kanatzidis, M. G. Ag_2Se to KAg_3Se_2: Suppressing Order–Disorder Transitions via Reduced Dimensionality. *Journal of the American Chemical Society* **2018**, *140* (29), 9193-9202.

(22) Li, B.; Wang, H.; Kawakita, Y.; Zhang, Q.; Feygenson, M.; Yu, H. L.; Wu, D.; Ohara, K.; Kikuchi, T.; Shibata, K.; Yamata, T.; Ning, X. K.; Chen, Y.; He, J. Q.; Vaknin, D.; Wu, R. Q.; Nakajima, K.; Kanatzidis, M. G. Liquid-like thermal conduction in intercalated layered crystalline solids. *Nature Materials* **2018**, *17* (3), 226-230.

(23) Jana, S.; Gabilondo, E. A.; Maggard, P. A. Two new multinary chalcogenides with $(Se_2)^{2-}$ dimers: $Ba_8Hf_2Se_{11}(Se_2)$ and $Ba_9Hf_3Se_{14}(Se_2)$. *Journal of Solid State Chemistry* **2024**, *329*, 124376.

(24) Srivastava, K.; Shahid, O.; Ray, A. K.; Deepa, M.; Niranjan, M. K.; Prakash, J. $Ba_8Zr_2Se_{11}(Se_2)$: The first polychalcogenide of the ternary Ba–Zr–Q (Q = S/Se/Te) system. *Journal of Solid State Chemistry* **2023**, *328*, 124344.

(25) Hansen, C. J.; Zak, J. J.; Martinolich, A. J.; Ko, J. S.; Bashian, N. H.; Kaboudvand, F.; Van der Ven, A.; Melot, B. C.; Nelson Weker, J.; See, K. A. Multielectron, Cation and Anion Redox in Lithium-Rich Iron Sulfide Cathodes. *Journal of the American Chemical Society* **2020**, *142* (14), 6737-6749.

(26) Grayfer, E. D.; Pazhetnov, E. M.; Kozlova, M. N.; Artemkina, S. B.; Fedorov, V. E. Anionic Redox Chemistry in Polysulfide Electrode Materials for Rechargeable Batteries. *ChemSusChem* **2017**, *10* (24), 4805-4811.

(27) Martinolich, A. J.; Zak, J. J.; Agyeman-Budu, D. N.; Kim, S. S.; Bashian, N. H.; Irshad, A.; Narayan, S. R.; Melot, B. C.; Nelson Weker, J.; See, K. A. Controlling Covalency and Anion Redox Potentials through Anion Substitution in Li-Rich Chalcogenides. *Chemistry of Materials* **2021**, *33* (1), 378-391.

(28) Sturza, M.; Han, F.; Shoemaker, D. P.; Malliakas, C. D.; Chung, D. Y.; Jin, H.; Freeman, A. J.; Kanatzidis, M. G. $NaBa_2Cu_3S_5$: A Doped p-Type Degenerate Semiconductor. *Inorganic Chemistry* **2013**, *52* (12), 7210-7217.

(29) Heremans, J. P.; Cava, R. J.; Samarth, N. Tetradymites as thermoelectrics and topological insulators. *Nature Reviews Materials* **2017**, *2* (10), 17049.

(30) Hohenberg, P.; Kohn, W. Inhomogeneous Electron Gas. *Physical Review* **1964**, *136* (3B), B864-B871.

(31) Kohn, W.; Sham, L. J. Self-Consistent Equations Including Exchange and Correlation Effects. *Physical Review* **1965**, *140* (4A), A1133-A1138.

(32) Kresse, G.; Hafner, J. Ab initio molecular dynamics for liquid metals. *Physical Review B* **1993**, *47* (1), 558-561.

(33) Kresse, G.; Hafner, J. Ab initio molecular-dynamics simulation of the liquid-metal--amorphous-semiconductor transition in germanium. *Physical Review B* **1994**, *49* (20), 14251-14269.

(34) Kresse, G.; Furthmüller, J. Efficiency of ab-initio total energy calculations for metals and semiconductors using a plane-wave basis set. *Computational Materials Science* **1996**, *6* (1), 15-50.

(35) Blöchl, P. E. Projector augmented-wave method. *Physical Review B* **1994**, *50* (24), 17953-17979.

(36) Perdew, J. P.; Burke, K.; Ernzerhof, M. Generalized Gradient Approximation Made Simple. *Physical Review Letters* **1996**, *77* (18), 3865-3868.

(37) Perdew, J. P.; Burke, K.; Wang, Y. Generalized gradient approximation for the exchange-correlation hole of a many-electron system. *Physical Review B* **1996**, *54* (23), 16533-16539.

(38) Krukau, A. V.; Vydrov, O. A.; Izmaylov, A. F.; Scuseria, G. E. Influence of the exchange screening parameter on the performance of screened hybrid functionals. *The Journal of Chemical Physics* **2006**, *125* (22), 224106.

(39) Togo, A. First-principles Phonon Calculations with Phonopy and Phono3py. *Journal of the Physical Society of Japan* **2022**, *92* (1), 012001.

(40) Skelton, J. M.; Burton, L. A.; Jackson, A. J.; Oba, F.; Parker, S. C.; Walsh, A. Lattice dynamics of the tin sulphides SnS2, SnS and Sn2S3: vibrational spectra and thermal transport. *Physical Chemistry Chemical Physics* **2017**, *19* (19), 12452-12465.

(41) Baker, C. L.; Lincoln, F. J.; Johnson, A. W. S. A low-temperature structural phase transformation in CuAgS. *Acta Crystallographica Section B* **1991**, *47* (6), 891-899.

(42) Yuan, B.; Zhu, W.; Hung, I.; Gan, Z.; Aitken, B.; Sen, S. Structure and Chemical Order in S–Se Binary Glasses. *The Journal of Physical Chemistry B* **2018**, *122* (50), 12219-12226.

SYNOPSIS: $NaBa_2M_3Q_3(Q_2)$ (M = Cu, Ag; Q = S, Se) were synthesized using solid-state methods and include the first reported structures in the Na-Ba-Ag-Q quaternary space. Mixed-chalcogen $NaBa_2Cu_3Se_{5-x}S_x$ compositions exhibit anion ordering and have both homonuclear and heteronuclear $(Q\text{-}Q)^{2-}$ anionic dimer units in the layered structure.